國 立 成 功 大 學

生 物 醫 學 工 程 研 究 所

碩 士 論 文

機器學習與深度神經網路
用於心臟電位影像重建

Solving Inverse Electrocardiographic Mapping Using Machine learning and Deep Learning Frameworks

研究生： 陳可維 Student: Ke-Wei, Chen

指導教授： 林哲偉 博士 Advisor: Che-Wei Lin

Department of Biomedical Engineering

College of Engineering

National Cheng Kung University

Tainan, Taiwan, Republic of China (R.O.C.)

Thesis for Master of Science

October, 2021

中華民國一百一十年十月

國立成功大學

碩士論文

機器學習與深度神經網路用於心臟電位影像重建
Solving Inverse Electrocardiographic Mapping Using Machine Learning and Deep Learning Frameworks

研究生：陳可維

本論文業經審查及口試合格特此證明

論文考試委員：林哲偉
許育吳
翁振勛

指導教授：林哲偉

系(所)主管：

（單位主管是否簽章授權由各院、系（所、學位學程）自訂）

中 華 民 國 110 年 10 月 2 日

機器學習與深度神經網路
用於心臟電位影像重建

陳可維[1]　　林哲偉[2]

國立成功大學生物醫學工程學系

摘要

心臟電位影像重建(Electrocardiographic imaging)是基於體表所測得之心電圖，重建心臟表面或內部的電位分佈的過程。此問題亦被稱為反向問題(Inverse Problem)。由於此問題在本質上無法得出唯一解，以及不容易針對體表與心臟間的電傳導性建模，目前針對此問題所發展出的方法，其準確度約 0.7(所重建的心電圖與實際心電圖之間相關系數之中位數)。本研究嘗試使用神經網路解決此問題，以增加模型的準確度。

本研究使用之兩組資料，一是來自於豬體表所量測之多個心電圖訊號，二是同時量測之豬心臟表面的心電圖。第一部分的研究，訓練與測試模型的資料皆來自同一之豬。所使用之神經網路有兩種。一是由數個全連接層(Fully Connected Layer FCN)所組成之神經網路，二是由長短期記憶(Long Short-Term Memory LSTM)神經網路所組成。第二部分的研究，我們將來源於不同的五隻豬之資料進行轉換，加以統合。接著我們使用卷積神經網絡(Convolutional Neural Network CNN)來建立模型。本研究使用留一驗證（leave-one-out cross-validation）作為模型準確度的驗證方法。

若比較重建的心臟表面心電圖與實際心電圖，在第一部分研究中，使用全連接層 FCN 之部分，整體的相關系數之中位數以及前四分之一與後四分之一的數值為 0.90 [0.68–0.96]。使用全連接層 LSTM 之部分則為 0.82 [0.54–0.93]。在第二部分研究，

[1] 研究生
[2] 指導教授

使用 CNN，整體的相關系數之中位數以及前四分之一與後四分之一的數值則為 0.74 [0.22–0.89]。

若比較重建的激發時間圖(activation map)，在第一部分研究中，使用全連接層 FCN 之部分，整體的相關系數之中位數以及前四分之一與後四分之一的數值為 0.86 [0.61–0.93]。使用全連接層 LSTM 之部分則為 0.52 [0.05–0.80]。在第二部分研究，使用 CNN，整體的相關系數之中位數以及前四分之一與後四分之一的數值則為 0.82 [0.67–0.93]。

若比較激發點位置誤差(localization error)，在第一部分研究中，使用全連接層 FCN 之部分，整體的距離之中位數以及前四分之一與後四分之一的數值為 10.4 [3.6–22.6] mm。使用全連接層 LSTM 之部分則為 18.5 [6.4–41.5] mm。在第二部分研究，使用 CNN，整體的相關系數之中位數以及前四分之一與後四分之一的數值則為 9.3 [3.4–17.0] mm。

本研究顯示，針對心臟電位影像重建，我們可以使用相對少量的資料解決。我們所達到的最佳結果為 0.74(所重建的心電圖與實際心電圖之間相關系數之中位數)。此外，本研究也顯示並不需要精確的座標資訊來重建心電圖。針對模型的準確性而言，在不同的豬隻與不同的量測結果之歧異度仍然很大。這可能與資料量相對較小有關，這可以在第二部分研究中看到。其整體準確度較佳，可能與其整合了所有的資料，其資料量較第一部分多有關。臨床應用部分，此研究顯示可使用非侵入性的體表量測心電圖，來找尋心臟的電刺激源點。此資訊可用於心室早期收縮病人之治療。

關鍵詞：心臟電位影像重建(Electrocardiographic imaging)、反向問題(Inverse Problem)、機器學習(Machine learning), 深度學習(Deep Learning)

Solving Inverse Electrocardiographic Mapping Using Machine learning and Deep Learning Frameworks

Ke-Wei Chen[1] **Che-Wei Lin**[2]

Department of Biomedical Engineering

National Cheng Kung University, Tainan 701, Taiwan, R.O.C.

Abstract

Electrocardiographic imaging reconstructs the heart surface as an electrogram using the potentials recorded from the body surface. This problem is called the inverse problem. Due to the ill-posed nature and the difficulty in modeling the conductive property of the body, currently, the overall accuracy for a reconstructed electrogram is only 0.7(median correlation coefficient for activation time map). This study tries to improve the model's accuracy using a neural network.

Electrocardiograms are simultaneously recorded from pigs' hearts and their body surfaces. For part I of the study, we trained and tested the model with the same pig. The neural network is composed of Fully Connected Neuro network (FCN) and Long Short-term Memory (LSTM) neural network. For part II of the study, we align the data from five different pigs by transforming the torso potential data into 2D data and transforming the epicardial potential data with a registration method. A Convolutional Neural Network is used to construct the model. We evaluated the method using leave-one-out cross-validation.

For the reconstructed electrogram in part I, the overall median of correlation efficient with the first to third quantiles are 0.90 [0.68–0.96] and 0.82 [0.54–0.93] for FCN and LSTM, respectively. In part II, the overall median of the correlation efficient with the first to third quantiles is 0.74 [0.22–0.89].

[1] Student
[2] Advisor

For the reconstructed activation map in part I, the overall medians of the correlation efficient with the first to third quantiles are 0.86 [0.61–0.93] and 0.52 [0.05–0.80] for FCN and LSTM, respectively. In part II, the overall median of the correlation efficient with the first to third quantiles is 0.82 [0.67–0.93].

For the localization error of the predicted pacing site in part I, the overall medians of the correlation efficient with the first to third quantiles are 10.4 [3.6–22.6] mm and 18.5 [6.4–41.5] mm for FCN and LSTM, respectively. In part II, the overall median of the correlation efficient with first to third quantiles is 9.3 [3.4–17.0] mm.

In conclusion, a neural network can be used to solve the inverse problem of ECGi with relatively small datasets. Our best result shows overall median of the correlation efficient to be 0.82. Our study also shows that a rough geometrical information of torso and heart may be enough to reconstruct the epicardial gram. Performance of the model is inconsistent between different recording and pig. This may be due to relatively small dataset and may improve with larger dataset. As shown in part II study, it has better result when model is trained with more data. In clinical setting, this study shows the potential to identify source of pacing site with non-invasive electro-cardiogram recorded from the surface, which can be applied to evaluation for patient with premature ventricular contractions.

***Keywords**:* Electrocardiographic imaging, inverse problem, Machine learning, Deep Learning

Acknowledgements

這個研究是我第一次接觸機器學習與深度學習，到現在仍能記得那時對這個工具的驚嘆與衝動。感謝林哲偉教授將我引入這個領域。回想一開始，還以為我的研究會天天待在研究室組電路，量 ECG。當林教授提出用所謂機器學習時，已還只認識一維函數的我，還想說，這怎麼可能。當用 Matlab 看到 trace 的結果時，仍能記得當時的悸動。

雖然在研究初期有了些結果，但到後來就遇到了一個很大的瓶頸。就是，沒有資料，而動物實驗對實驗室來說，也沒有足夠的經驗與能力來執行。加上中間休學一年參與 STB 計畫到美國一年，研究於是陷入停滯，一直在繞圈圈沒有太多實質的進展。

直到在美國遇到另一位 STB 學員陳馥郁，她在紐西蘭奧克蘭大學(Auckland university)取得醫學工程博士學位。而我正好久聞有位 Laura Bear 也是在那裏做 ECGi 的研究，並有一筆資料。於是請馥郁幫忙牽線，先是詢問了 Laura Bear 的指導教授 Bruce Henry Smaill。感謝他進一步幫忙牽線連絡上已在法國擔任研究員的 Laura Bear。她收到我的 email 後，很爽快地就將所有的原始資料分享。這讓我如獲至寶，有了這份資料，才有了後續的研究成果。

另外由於我大部分時間仍在工作，不在學校與實驗室，感謝研究室的同學平時的幫忙。感謝王意雯、謝侑良、林欣蓉、顏毓秀等夥伴，有你們，這篇論文才能順利完成。

Table of Contents

List of Tables

List of Figures

List of Abbreviations

Abbreviation	Meaning
2D	Two-dimensional space
1D	One-dimensional space
ECGi	Electrocardiographic imaging
CC	Correlation Coefficient
CC_{AT}	Correlation Coefficient of Activation Map
CC_{time-k}	Correlation Coefficient of potential across all time step at epicardial lead k
μ_M	mean values across all measured potential or activation time
μ_R	mean values across all reconstructed potential of activation time
FCN	Fully Connected Neural
LSTM	Long Short-term Model
CNN	Convolutional Neural Network
AT	Activation Time
V_t	Potential at time step t
ECG	Electrocardiograms
mV	microvolt
ms	microsecond

Chapter 1

Introduction and Background

1.1. Inverse Electrocardiographic Mapping

Studying the electrical activity of the heart is important for clinicians to make diagnoses or for monitoring. By placing electrodes over the body surface, such as the chest and limbs, we can reveal the electrical activity remotely and non-invasively. The graph data we gather is referred to as electrocardiography (ECG or EKG). The recording can also be invasive, gathering potential information directly from the endocardium through a catheter. The information gathered is referred to as an intra-cardiac electrogram. By combining the electrogram with its geometrical location, we can map the results to the endocardial surface, which is referred to as electroanatomical mapping.

Monitoring the heart's electrical activity via body surface recordings is an indirect measurement method. For example, the typical 12-leads ECG system only shows 12 time series data with a rough direction for each potential recording; therefore, it is difficult to locate the anatomical location of abnormalities. It will be very helpful if we could directly see the heart potential with its geometrical location over the heart. There have been many attempts to map body surface recordings to the heart; this process is called inverse electrocardiographic mapping. Usually, the target of mapping is the potential over the heart surface (epicardial potential). This mapping can also be referred to as electrocardiographic imaging (ECGi).[1]

ECGi is currently use for heart arrythmia, since it can provide the geometrical information of the electrical abnormality of a heart. Currently, atrial arrhythmias(Af) is the most common arrhythmia that incorporate the ECGi into the workflow for treatment. For example, it can be use to identify the specific patterns of activation, which will help the physician to plan the ablation before sending the patient to the table. ECGi can also help physician to find the source of pacing source. This will be useful for the premature ventricular contraction(PVC) ablation. Furthermore, ECGi has also been used to recognize the potential slow conduction area of heart. This information can be used to stratify risk of ventricular arrythmias.[2]

1.2. The importance of inverse electrocardiographic mapping

For ablation of the arrhythmia source, it is important to identify the location of the abnormal rhythm. Traditionally, this is done by electroanatomical mapping, which is done by recording the potential information of the endocardium through a catheter. Currently, physicians need to perform mapping directly by repeatedly touching the endocardium with a catheter, which can be time-consuming. Inverse electrocardiographic mapping can reduce the time and provide opportunities for pre-operation evaluation. This has already been used in the clinical field for pre-operation evaluation or quick analyses during operations. One example is the ECGi system (CardioInsight, Medtronic Inc, Minneapolis, MN).

1.3. Traditional Methods

Traditional methods for solving the problem are generally composed of two steps.[3] The first is call forward problem formulation, which uses the heart as an electromagnetic source. A cardiac source model can be constructed using Maxwell's equations and geometrical information. It is usually put in a matrix *A*:

$$\emptyset_T = A\emptyset_H \quad (1)$$

$\emptyset_T$ is the potential over the body surface in vector form, $\emptyset_H$ is the potential over the heart surface, and A is the matrix that transforms the heart surface potential into the body surface potential, which usually requires geometrical information of the body and heart. The modeling of matrix A is usually referred to as a forward problem.

The second step is to perform an inversion of matrix A.

$$\emptyset_H = A^{-1}\emptyset_T \quad (2)$$

A^{-1} is the inverse matrix of A. This problem is usually referred to as an inverse problem.

Multiple methods has been developed based on this framework. The source of electrical activity can be directly modeled as the epicardial potential; it can also be modeled from the activation time. The first method is called the potential-based model and the second is the activation-based model. The Boundary Element Method (BEM) is used to solve matrix *A*, but it required a mesh from the 3D geometry, which could sometimes be time-consuming and can introduce mesh-related defects. The meshless method of fundamental solutions (mMFS) was developed to solve this problem. [4] We can simply model the medium between the heart and body surface as a medium with consistent conductivity, which is

referred to as homogeneous modeling. We can also consider the different conductivity within different tissue, such as lung, muscle, and fat; this model is referred to as an inhomogeneous model.

1.4. Problems faced in current methods

Despite the simplicity of this modeling method, it has many problems. For one, the inversion of matrix *A* is not unique. Moreover, the inverse problem is ill-posed, which means that the prediction is subject to noise in the body surface potential; it required further regularization [3]. Those abovementioned problems may explain why the currently reported accuracy of the reconstructed potential is still not ideal; see Table 2. There are different ways to obtain validation. For the torso tank experiment, which used a tank with body surface and dog heart as the potential source, the median correlation coefficients can be up to 0.8 (median correlation coefficient for electrogram). For an in-situ animal study, the potential from the heart and body surface are simultaneously recorded from animals such as dogs or pigs. The current accuracy for this study is around 0.7 (median correlation coefficient of activation time map) [5]. For validation in a clinical setting, the current result is also around 0.7 (median correlation coefficient of activation time map) for paced rhythm. The results are even worse for normal QRS, which is 0.03 (median correlation coefficient of activation time map).[6]

1.5. Neural network for prediction

In recent years, neural networks have proven to be a useful tool for modeling data with complex relationships. Currently, only a few attempts have been conducted to solve the inverse problem with a neural network. In one study [7], data is collected from a torso tank setting using Time Delayed Neural Nets and Feed Forward Neural Nets (FFNNs). Their results are not very ideal with most having a median correlation coefficient <0.5. There are two main problems; the first of which is overfitting. The model converges well in the training round but performs poorly in the testing round. The second problem is how to apply different subjects with different heart and body geometry. This problem exists because the training data does not contain information from the geometry. [7]

In our study, we will build our model directly from data collected from an *in situ* animal study. To build a model that can be applied to subjects with different geometries, we will create a data registration method to incorporate the geometric information into the data sequence.

Chapter 2

Material and Methods

2.1 Overall design of the study

The open dataset for the ECGi study is quite limited. In search of the internet, there is only one website (Experimental Data and Geometric Analysis Repository EDGAR [8]) that store the electrocardiogram date, and is open to public. Even in the repository, the amount of data is limited. Usually, only partial recording is provided. Out of luck, we have been to able to make contact with Laura Bear who the main collector of a dataset. She performed the animal study to acquire this dataset during her doctoral study in Auckland university in new Zealand. With this dataset in hand, we design our study as shown in Figure 1. Part I indicates the study that trains data only for the same pig. Part II study uses data from all four pigs and has an additional step (Registration of electrogram data) that transforms the original data into a uniform data format. (Metrics) Models are evaluated in three ways. One is the correlation coefficients for the reconstructed electrogram to the recorded one. One is the correlation coefficients for the AT map derived from the reconstructed and recorded electrogram. CC correlation coefficients. AT map activation time across all epicardial nodes.

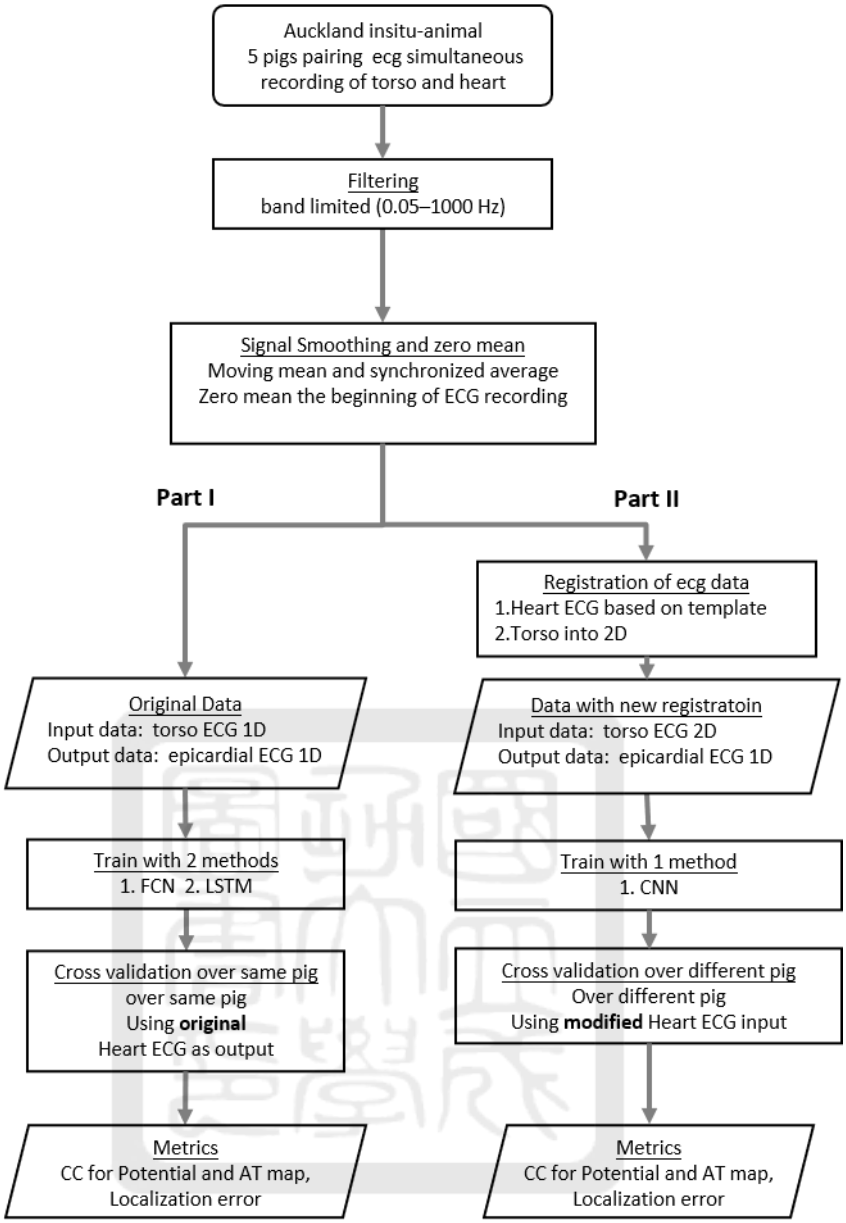

Figure 1 Overall study process.

2.2 Data collection

Previous literature illustrates the details of the data collection process. [9] A short summary of the experiment is provided below. There are two sets of data being collected. One is electrograms recorded from a vest wrapped around a pig. The electrograms record the potential change in the pigs' body surface. Another set is electrograms recorded from a sock wrapped around the heart. The electrograms show the potential changes of the heart surface, as shown in Figure 2. (On the left) Demonstration of a pig's heart surrounded by a sock with multiple electrode. (In the middle) Demonstration of a pig's trunk with heart in

the middle. The stripes indicate the array of electrode over body surface. (On the right) The position of electrode and geometrical information of the heart and body is extracted from MRI image. The figure is adapted from [5]

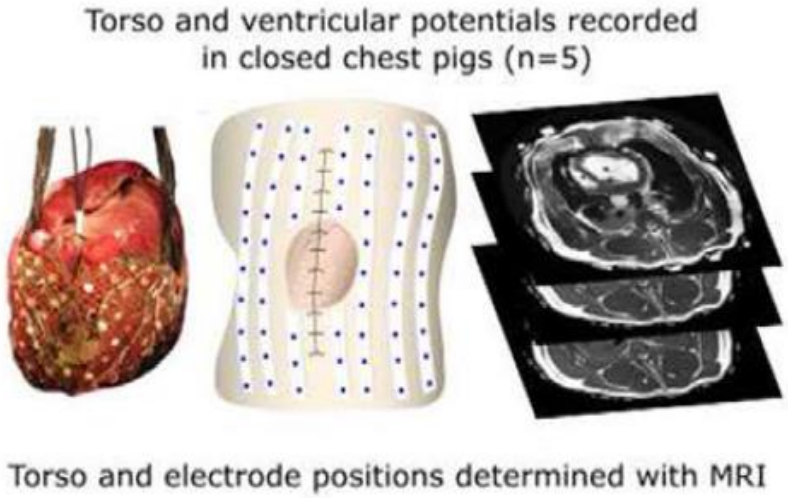

Figure 2 Electrodes over pig's heart and torso surface

To place the recording leads, five anesthetized pigs (around 30–49 kg) underwent a midline sternotomy. A sock containing 239 unipolar silver wire electrodes was then placed around the heart. After the procedure, the chest was closed and air was expelled from the lungs. Flexible stripes containing electrodes were placed inside a vest that was wrapped around the pig's torso. The epicardial and body surface potentials were then recorded simultaneously. The electrocardiograms are then recorded with a sampling rate of 2 kHz and a bandwidth limitation of 0.05–1,000 Hz. The electrograms are further smoothed by moving the mean and synchronized average. To reduce the effect of potential shifting, we synchronously shifted all electrograms so that the mean of all potential values across all nodes at the beginning of the cycle equals zero.

There are three pacing types: sinus rhythm, epicardial pacing, and endocardial pacing. The pacing sites are all across the heart. Overall, there are 76 recordings, each of which contains around 10–20 beats. Table 1 shows the composition of the data. About 10–20% of the leads on the vest took poor recordings. We used linear interpolation to fill up the missing data.

2.3 Final data used in the study

The data is further smoothed by synchronized average and moving mean. After this process, each pacing site or sinus rhythm contains only one cycle of electrocardiogram. The number of leads over the torso surface is around 150–170 and the total number of epicardial leads is 239. Table 1 shows the number of recordings from different pacing sites and recording leads. Over the shaded area, number of recordings with different pacing sites or rhythms. Over the button 2 rows, number of recording leads over the torso and epicardial surface. Note that the whole electrogram cycle is used for model training and testing. Unlike most studies, only the potential during ventricular activation is used.

Table 1 Number of recordings from different pacing sites and recording leads.

	Pig 1	Pig 2	Pig 3	Pig 4	Pig 5
Sinus rhythm	1	1	1	1	1
Endocardial pacing	4	5	0	12	10
Epicardial pacing	8	18	4	0	10
Total number	13	24	5	13	11
Torso lead number	158	150	171	165	170
Epicardial lead number	239	239	239	239	239

Since each pig has a different experiment setting, there is no consistency regarding the number of recording leads over the torso and different leads are set at different geometrical locations. We can train the model directly from the data but the model may only apply to data with the same experimental setting. Thus, we divided the experiment into two parts. For the first, we only considered the problem within each individual pig and we built the model only for the same pig. For the second part, we incorporated a registration method to unify data from different pigs.

2.4 Part I study: without Considering the Geometry

2.4.1 Model selection

Two methods are used to establish a model. One is a neural network with a few fully connected layers using Hyperbolic Tangent as an activation function, as shown in Figure 3. Another is the Long Short-term Memory (LSTM) model, the structures of which are shown in Figure 3. Over the left part, it shows the fully connected model used in this study. Over

right side, it shows the LSTM model used in this study. The input size ranges from 1x150–165 depending on the ECG recording vest used for different pigs.

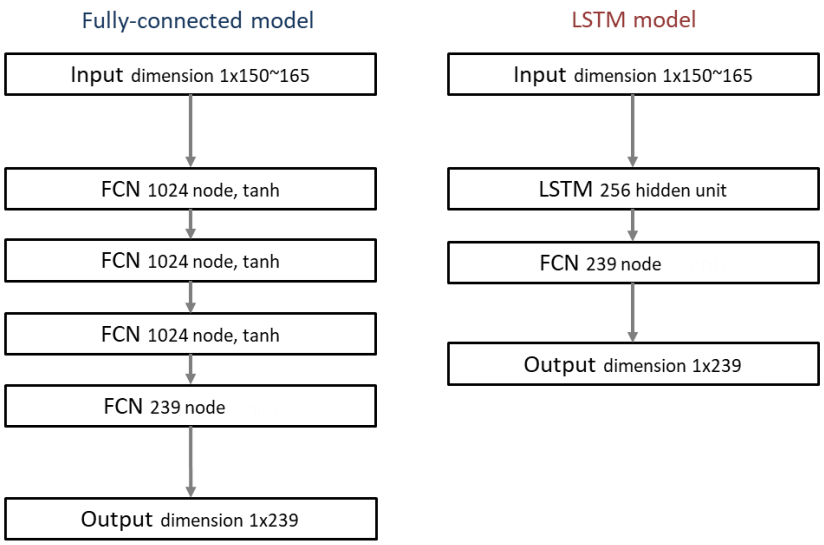

Figure 3 Models used in cross-validation over data in the same pigs in Part I study

2.5 Part II study: Add Geometrical Information

2.5.1 Torso node registration

The locations of torso leads are projected to a cylinder surrounding the torso. Then, the surface of this cylinder is used as a sampling plane to produce a 2D image as shown in Figure 4. The torso node geometry data is first centered on the geometric origin and then the nodes are projected to a cylinder surface surrounding the torso. The nodes' distance h to the x–y plane will then become the vertical distance. The degree θ between the y axis and the node will then be the horizontal distance. The torso node geometry data is first centered on the geometric origin, and then the nodes are projected to a cylinder surface. θ is degree from the y axis to the node and h is the height from the x–y plane to the node.

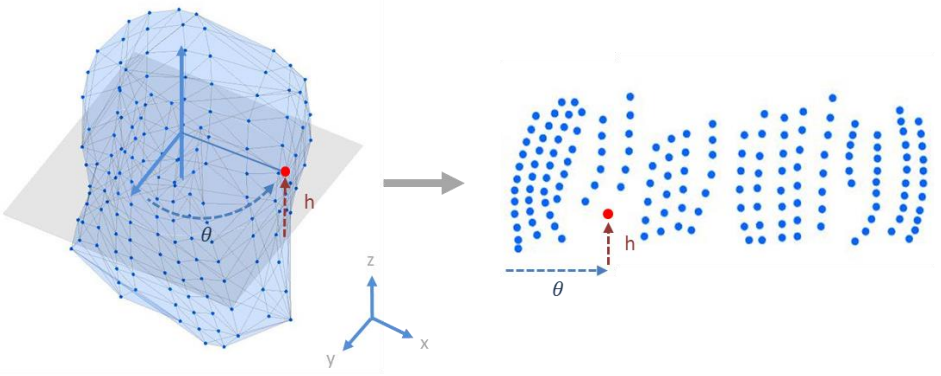

Figure 4 Registration of the torso node to the 2D plane.

In figure 5, it shows the results of all the transformation from all the pigs. The 3D view shows the original 3D distribution of the torso node, where the ECG is recorded. The 2D scatter plot shows the distribution of the node after the projection to a cylinder. The double arrow indicates the region that belongs to the anterior, posterior, top, or bottom area of the torso.

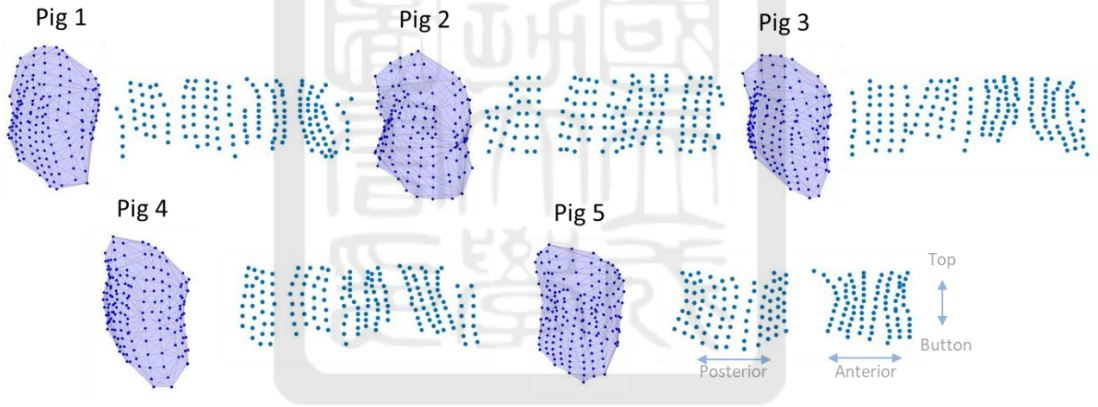

Figure 5 Results of torso nodes registration to the 2D plane.

2.5.2 Transforming 1D data into 2D

Bilinear interpolation is used for the sampling method. The sampling points are a grid of width 90 pixels and height 30 pixels, as shown in Figure 6. Over the left side part, it shows normalized torso node distribution. Node color is mapped to the potential value. Over the right side part, it shows grids with 30x90 pixels are merged with the scattered node. Nodes in the grid are used as sampling points. The potential values are computed by the bilinear interpolation method. The potential value shown here is data from pig1's first recording at 90 ms after pacing.

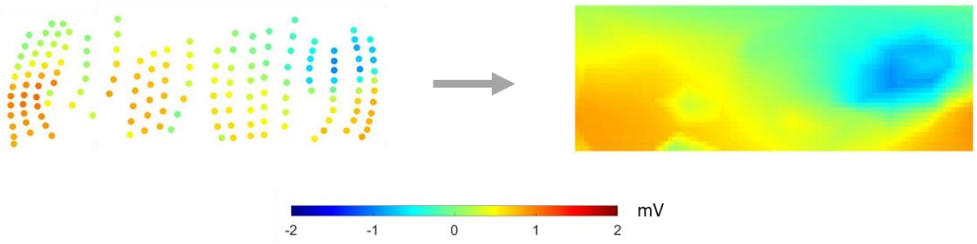

Figure 6 Use the bilinear interpolation to transform data into 2D.

2.5.3 Epicardial surface node registration

For the epicardial node, the original data is a sequence of electrocardiograms. Each pig has their own sequence and each electrocardiogram is from a different recording location; there is no geometrical correlation to the sequence of leads.

To unify the data across all pigs' data, we invented a way of translating the electrocardiograms into the same sequence and number. The overall concept is that we projected the epicardial node to the x–y plane and used a template node distribution as the sampling point over the projected node. Since the sequence of nodes in the template is fixed, we can transform the original data into 1D data in which the data sequence has a fixed geometrical order; Figure 7 shows this process.

As shown in Figure 7 the node at the tip of the heart over the apex is used as the origin in the coordinate system. The epicardial node is projected to the x–y plane first. The result will be a scattered map containing the orientation of the node to the body. However, some nodes may overlap with each other since they can be on top of each other. To have a more evenly distributed map, we extend the nodes' location along the vector from the origin to the nodes. The result will be a 2D scatter map where the location indicates the orientation of nodes and the distance to the tip of the nodes in the original 3D space.

Since different hearts have different shapes, the distributions of the nodes are not circular but oval. To further normalize the distribution, we further chop the map into pies. The radius of each pie is the radius of the node that is the most distant from the center $\boldsymbol{L}$. The nodes inside the pie are further shrunk with same ratio toward the center, so that all nodes will be within a smaller pie with radius $\boldsymbol{R}$. After this process, all nodes will be within a circular area with radius $\boldsymbol{R}$. When the arc of the pie is set to 30°, it means that the whole scatter plot is divided into 12 pies;

Figure 8 shows the epicardial registration results from the four pigs. The apex of the heart is used as the origin of the coordinate system. The node is then projected onto the x–y plane at n and then the node is extended along the vector between the tip and n until its distance between origin and node is r. r is the distance between the origin and the epicardial node; the final location is n' on the x–y plane. The scatter plot is further shrunk to a circular area by dividing the map into pie-shaped sections. From each section, find the node M with the maximal radius L and then shrink this node concentrically to a position with radius R. For the rest of the nodes in this pie area, reduce their radius so that the ratio of the new radius to the old radius is retained (equal to L/R). The arc of the pie area in this figure is 30°.

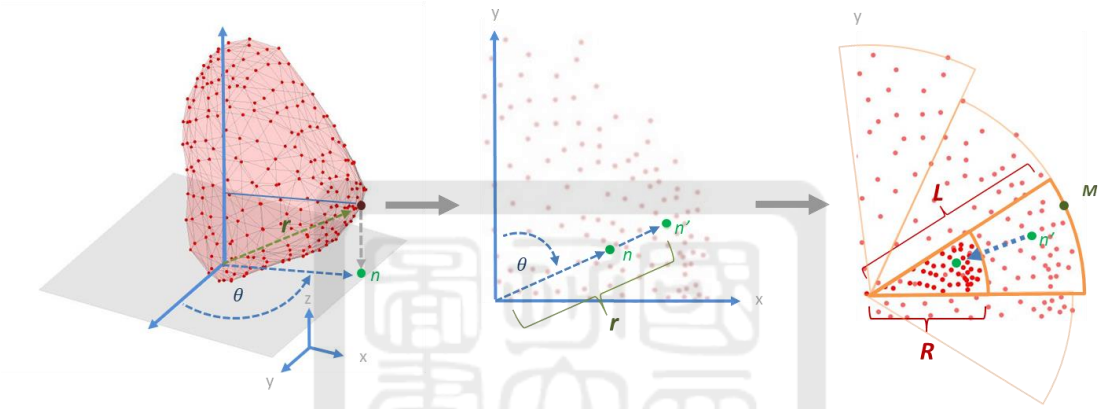

Figure 7. Registration of epicardial notes to the 2D plane.

In Figure 8, it shows the result of all the transformation from 5 pigs. Over the top row, original 3D distribution of the epicardial nodes. Over the middle row, first registration of the nodes. Over button row, further transformation of the nodes into a circular area.

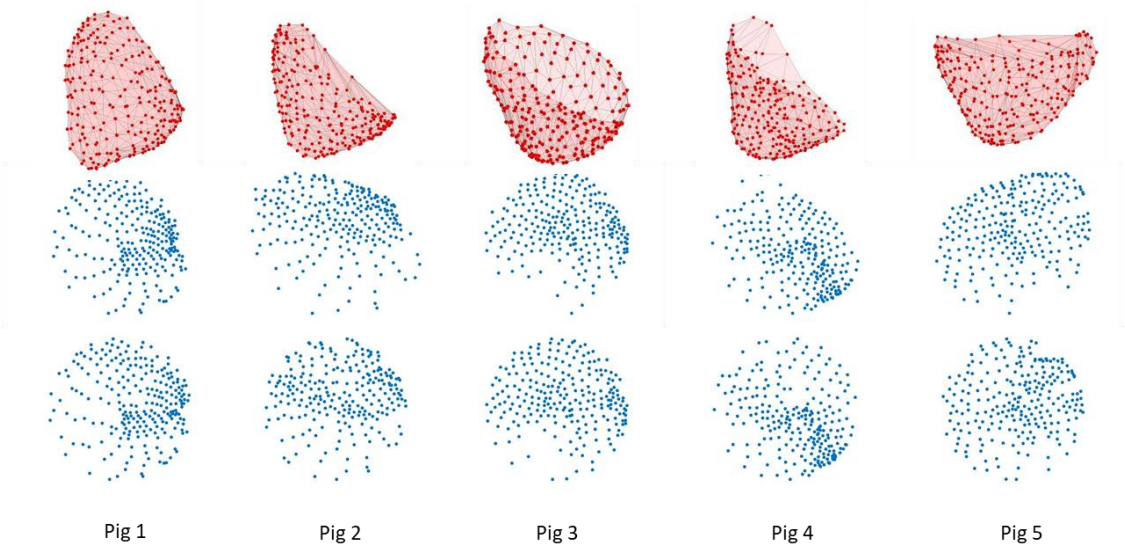

Figure 8 Results of epicardial node registration to the 2D plane.

2.5.4 Transforming 1D data into 1D data with the same geometrical sequence

Each pig during the experiment has their own sequence. After epicardial node registration, we can map the potential to the 2D scatter plot. We established a template with 165 nodes; the choice of location is rather arbitrary; we used seven layers of circles to cover the region of the 2D scatter plot. These 165 nodes are then used as sampling points to obtain the potential values. We used bilinear interpolation to acquire data, which is then further transformed into 1D data based on the template's node sequence. Here, the sequence we use is to put the first node at the center and then gradually go outward in a clockwise pattern. Since the sequence is fixed, even different pigs with different node sequences will have similar geometric sequences, as shown in Figure 9. Over the left most part, the first 10 nodes of the original potential data sequence 90 ms after pacing. The left scatter plot shows all epicardial nodes after the new registration. The bigger nodes are those 10 examples. The small purple nodes are the sampling locations of the template. The right scatter plot shows the results from sampling over the location on the template. The bigger nodes are the first 10 nodes of the template. Over the right most part, the first 10 nodes of the potential data after transformation. The potential values shown here are data from pig1's first recording at 90 ms after pacing.

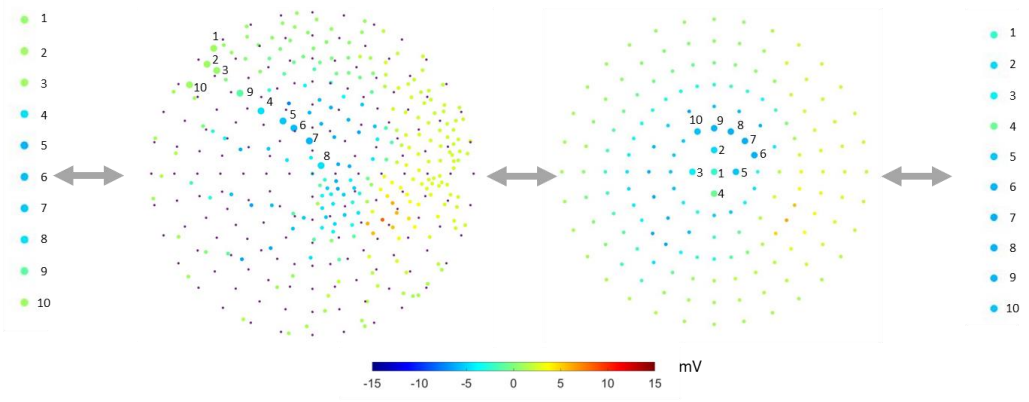

Figure 9. Transformation of 1D data by resampling with the new registration.

The overall data flow of part II will be as follows:

1 Transform the 1D data of the epicardial potential into a 2D scatter plot.

2 Use a template with 165 nodes to sample the potential.

3 Train the model that is output in the form of 165 1D sequences.

4 During testing, the output of the model is transformed back into the original sequence of epicardial potential by sampling the potential using the 2D scatter plot location.

2.5.5 Model selection

We used a simple neural network composed of three layers of a Convolutional Neural Network (CNN). The average pooling layer is also used, as shown in Figure 10. In the figure, filter 32 indicates that the output depth of the CNN layer is 32. As for tanh is the hyperbolic tangent that is used as an activation function. Hyperbolic Tangents are used as the activation function.

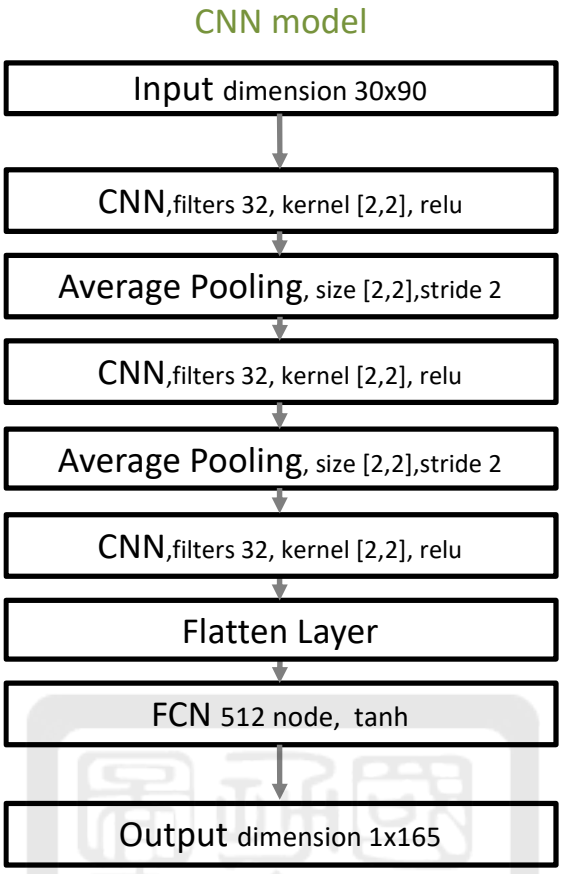

Figure 10. The Model used in cross-validation for different pigs in part II study

2.6 Model evaluation

2.6.1 Leave-one-out cross-validation.

In part I, when no geometry is considered, one full electrocardiogram cycle is the most meaningful representation of the heart activity, we chose each recording as single observation. Each recording takes turns being used as validation data while the rest is used as training data. For example, if there are 13 recordings from one pig, each recording will take a turn to be used as a validation set while the rest will be used as a training set; there are 13 trained models in total.

In part II, each pig has their own geometry. To show how the model performs with different geometry, the whole set of recordings from each individual pig are used as a single data unit. Each pig's data takes a turn being used as the validation data while the rest of the data are used as training data. For example, there are 61 recordings from four pigs and 13 recordings from pig 1. For the first cycle of cross-validation, 13 recordings from pig 1 will

be used as validation data while the remaining 48 recordings will then be used for training. There will be four trained models after cross-validation.

2.6.2 Evaluation metric: potential prediction

The correlation coefficient (CC) is used to evaluate the predictions of electrocardiograms for individual leads across all time steps. The CC at electrode k is defined as follows:

$$CC_{time-k} = \frac{\sum_{i=1}^{t}\left(V_M^i - \mu_M\right)\left(V_R^i - \mu_R\right)}{\sqrt{\sum_{i=1}^{t}\left(V_M^i - \mu_M\right)^2}\sqrt{\sum_{i=1}^{t}\left(V_R^i - \mu_R\right)^2}} \quad (1)$$

V_M^i and V_R^i are the potential at electrode k for measured (M) and reconstructed (R). t is the length of samples (sequence being recorded) μ_M and μ_R are the corresponding mean values across all samples.

Each recording will have 239 correlation coefficients since there are 239 epicardial leads and thus 239 recordings. For representation, we will only show the mean of all correlation coefficients across these 239 nodes.

2.6.3 Activation time reconstruction and pacing site localization

Potential reconstruction is only the first step in monitoring heart activity. To show the potential use of ECGi, we try to reconstruct the activation time and later predict the initial pacing site.

The activation time (AT) is often used to determine the source of pacing. The definition of AT at electrode k is as follows:

$$AT_k = \underset{t}{\operatorname{argmax}}\left(-\frac{V_{t+dt} - V_t}{dt}\right) \quad (2)$$

$V_{t+dt} - V_t$ is the potential difference after one time step at the *t*-th sample. The activation time will be the time step that has the maximal voltage decline in one-time step. In our study, dt is set to one sampling time 0.5 ms. The node that has the smallest activation time will then be predicted as the pacing site.

2.6.4 Evaluation metric: activation time

The correlation coefficient (CC) is also used to assess the accuracy of the predicted activation time, shown as follows:

$$CC_{AT} = \frac{\sum_{i=1}^{N}\left(AT_M^i - \mu_M\right)\left(AT_R^i - \mu_R\right)}{\sqrt{\sum_{i=1}^{N}\left(AT_M^i - \mu_M\right)^2}\sqrt{\sum_{i=1}^{N}\left(AT_R^i - \mu_R\right)^2}} \quad (3)$$

AT_M^i and AT_R^i are the activation time at electrode i for the measured (M) and reconstructed (R) value, N is the number of leads, and μ_M and μ_R are the corresponding mean values across all activation times. The activation times are further smoothed by incorporating the global activation fields. [10]

2.6.5 Evaluation metric: localization error

Activation times are used to find which node activates first. The node with the smallest activation time is chosen as the initial activating node. The localization error will be the Euclidean distance between the node identified by the recorded potential and the node by the reconstructed potential. We did not use the real pacing site to calculate the localization error; one reason for this is that we do not have the exact pacing site location for the endocardial pacing data. For another, the pacing site predicted from the recorded electrogram is not the same as the real pacing site. To simplify the analysis, we used the pacing site derived from the recorded electrogram as the ground truth.

Chapter 3

Results

3.1 Potential visualization

Figure 11 shows an example of the potential visualization. From the top row to the bottom row, the figure shows the potential from three-time steps. The top row is during the initial depolarization, the middle row is during the late depolarization process, and the bottom row is the repolarization phase.

In Figure 11, the figure shows the potential from three-time steps from top to bottom. In the first column, electrogram of the recorded and predicted potential. The vertical red line indicates the time step. In the second column, it shows visualization of the torso potential. In the third column, it shows potential from the torso lead recording after 2D transformation. In the fourth column, it shows visualization of the epicardial potential. In the fifth column, it shows epicardial node potential after transformation into a template. In the sixth column, it shows visualization of the reconstructed epicardial potential. In the fourth column, we show the epicardial node potential after its transformation into a template. The rightmost column shows the potential being reconstructed.

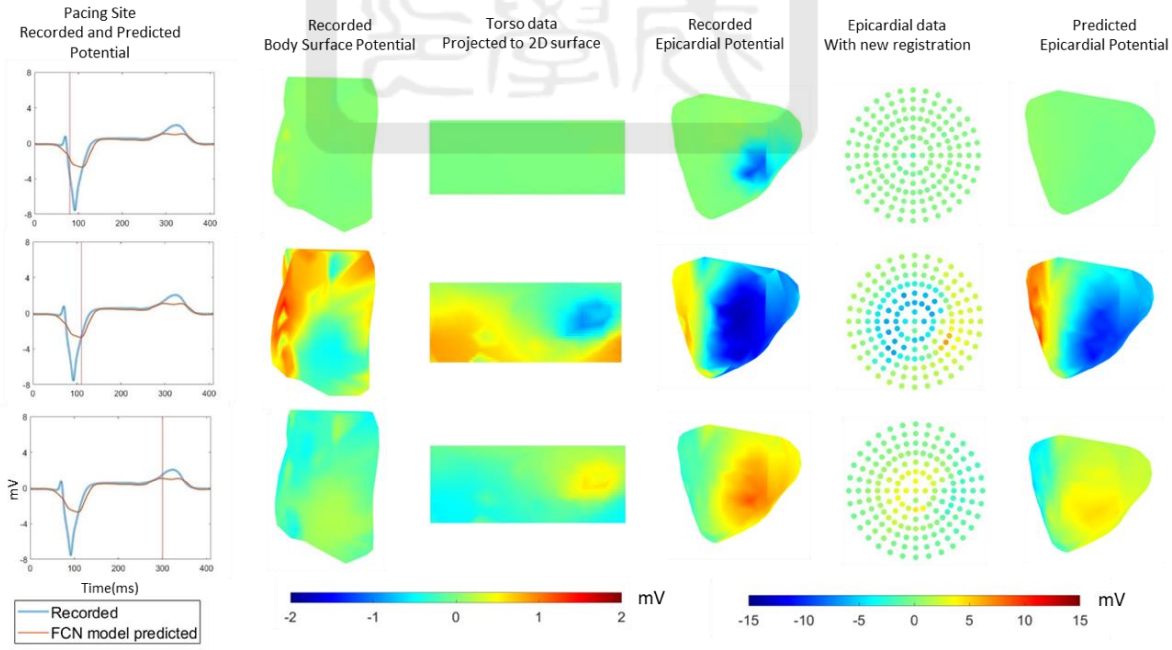

Figure 11, Example of potential visualization.

In Figure 12, the corresponding correlation coefficients are shown in the right upper part of the sub-figure. The testing data shown here is the first recording from pig 2. In the figure, FCN indicate prediction result from a fully connected neural network for the same pig cross-validation. LSTM indicate prediction result from the Long Short-term Memory model for the same pig cross-validation. CNN indicate prediction result from the convolutional neural network for different pig cross-validation.

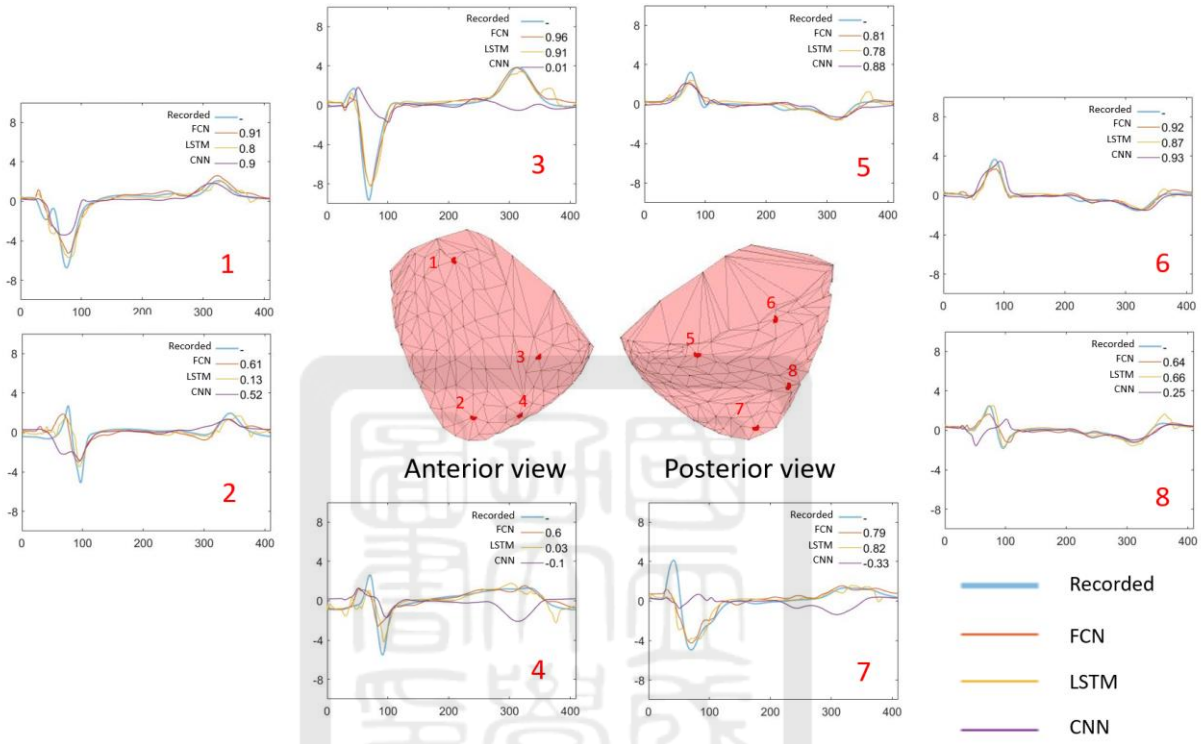

Figure 12 Examples of epicardial site electrograms (Recorded and Predicted).

3.2 Median Correlation Coefficient

Figure 13 shows the cross-validation result. For example, the dot in the figure over Part I from the FCN model testing result represents one of the cross-validation model test results. The dot represents the median correlation coefficient across all epicardial nodes CC_{time-k} as indicated in formula (1). For another, the model trained from pigs 2–4 is tested on the data from pig 1. Each recording will have one median correlation coefficient so there are 13 dots shown on part II from the CNN model first strip of dots. In the left side figure, cross-validation results using data from the same pig. In the right-side figure, cross-validation results using data from all pigs. Each dot represents the median correlation coefficient across 239 epicardial nodes.

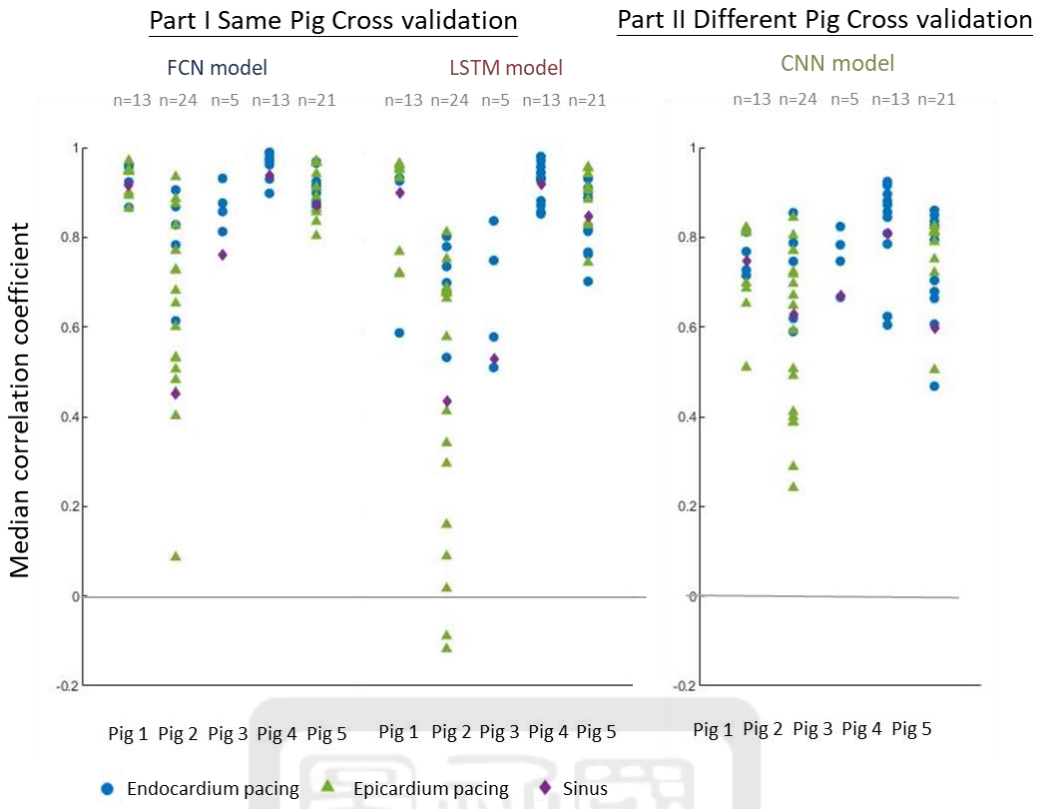

Figure 13 Cross-validation results

The results show that when considering only data from a single pig, the performance is quite varied. For example, the Fully-connected neural network (FCN) and Long Short-term Memory network (LSTM) performed well in pigs 1 and 3 with median correlation coefficients >0.8. If we accumulate all correlation coefficients from all results, the overall median of the correlation coefficient with the first to third quantiles are 0.90[0.68–0.96] and 0.82[0.54–0.93] for FCN and LSTM, respectively.

When combining all data, the overall performance is poorer. If we accumulate all correlation coefficients from all results, the overall median of the correlation coefficient with the first to third quantiles is 0.74[0.22–0.89]. This is shown in the right-side part of Figure 13.

3.3 Activation Time Correlation

Figure 14 is an example of an activation time map. The darker areas indicate a shorter activation time. From the figure, we can also note that even the activation time derived from the recorded electrocardiogram cannot find the real pacing site. The recording here is from pig 2. Over the left upper subplot, the activation map is derived from the recorded

electrogram. The spots represent one node over the epicardial surface. The colors indicate the value of the activation time. Over the right upper subplot, the activation map is derived from the electrocardiogram reconstructed by Fully Connected Neural network model. Over the left lower subplot, the activation map is derived from the electrogram reconstructed by Long Short-term Model. Over the right lower subplot, the activation map derived from the electrogram is reconstructed by Convolutional Neuro Network model. Green triangle shows the real pacing site in the experiment. Light Blue triangle shows predicted pacing site that has the lowest activation time.

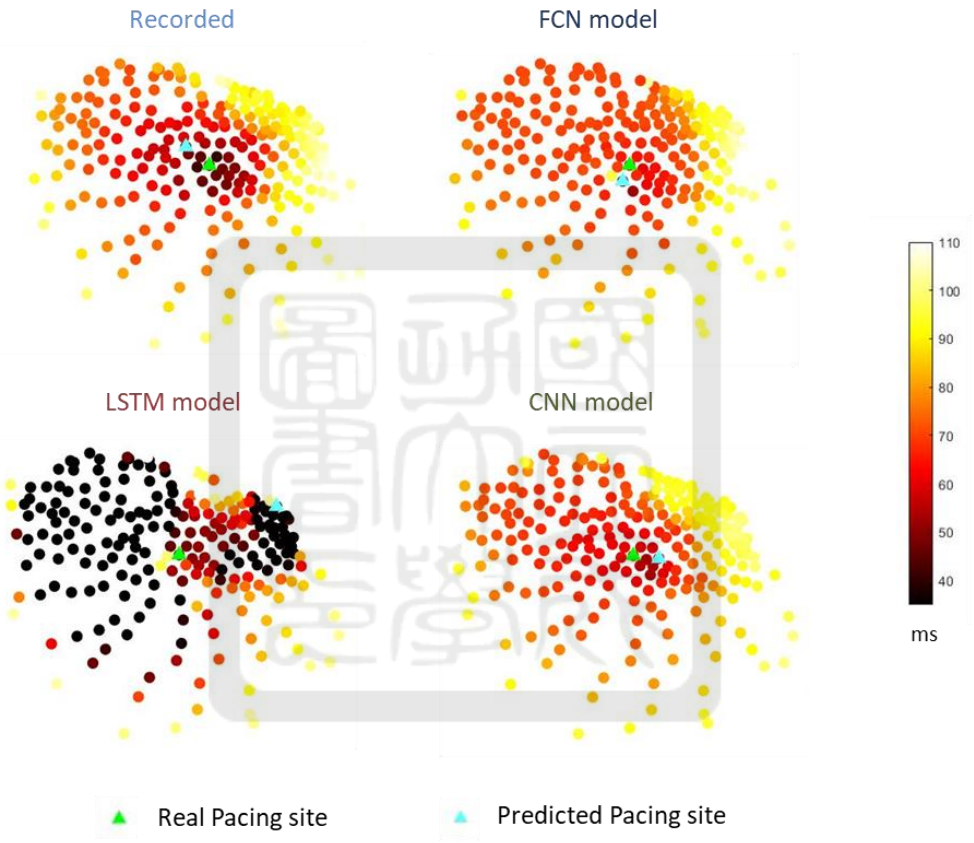

Figure 14 Examples of Activation Time Maps shown in the Scatter Plot.

The activation time map from the recorded data is compared with that from the reconstructed data as shown in Figure 15. Over the left side part of figure, it shows the correlation coefficient of the activation time map over the validation data in cross-validation. Over the left side part of figure, it shows correlation coefficient of the activation time map over all validation data in cross-validation. Each dot represents the correlation coefficient between the activation time map from the recorded data and the reconstructed data.

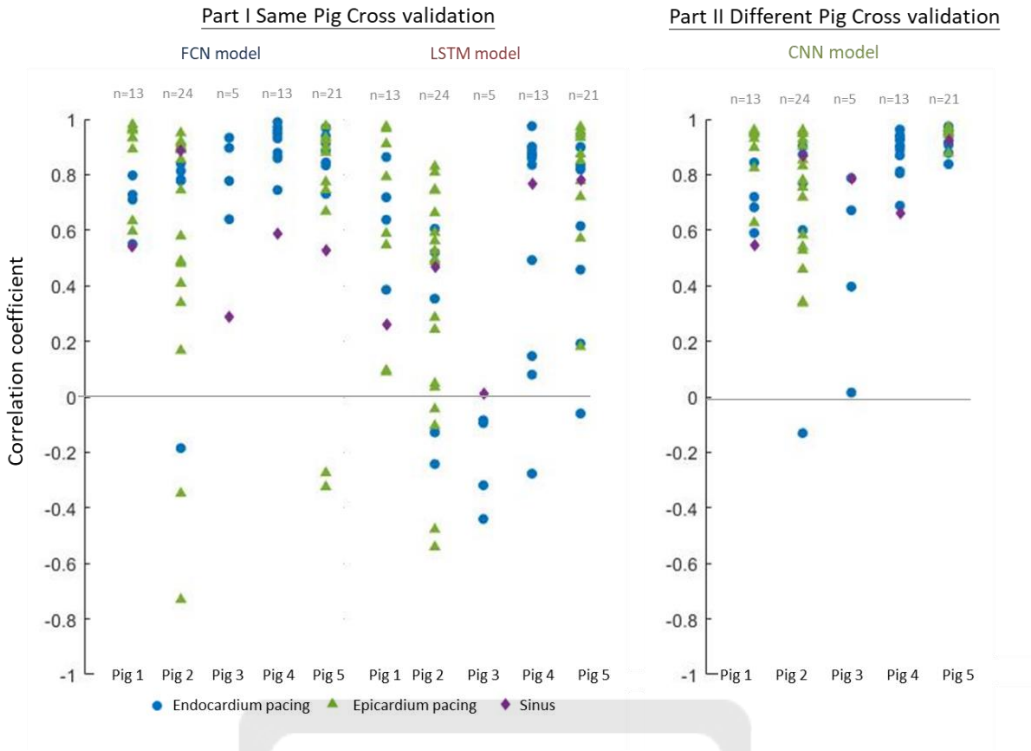

Figure 15, Correlation Coefficients between the Activation Time map derived from the recorded and reconstructed electrogram.

The result from the part I study shows a great variation amount for different data, while some of the data can show a correlation coefficient of up to 0.9, a lot of the data show negative correlation. The overall median of all correlation coefficients with the first to third quantiles are 0.86 [0.61–0.93] and 0.52 [0.05–0.80] for the FCN and LSTM models, respectively. The part II study, which combines all available data and shows much better performance with only one result below 0. The median of all correlation coefficients with the first to third quantiles is 0.82[0.67–0.93].

3.4 Localization error

Figure 16 shows the localization error from different cross-validation results. The results from the part I study show a great variation amount for different data, some locate the exact same node with the initial activation while some are around 60 mm apart. The median of all localization errors and first and third quantiles are 10.4 [3.6–22.6] mm and 18.5 [6.4–41.5] mm for the FCN and LSTM model results, respectively.

The performance is much better for the results from the part II study. All the localization errors and the first and third quantiles of all localization errors are 9.3[3.4–17.0] mm.

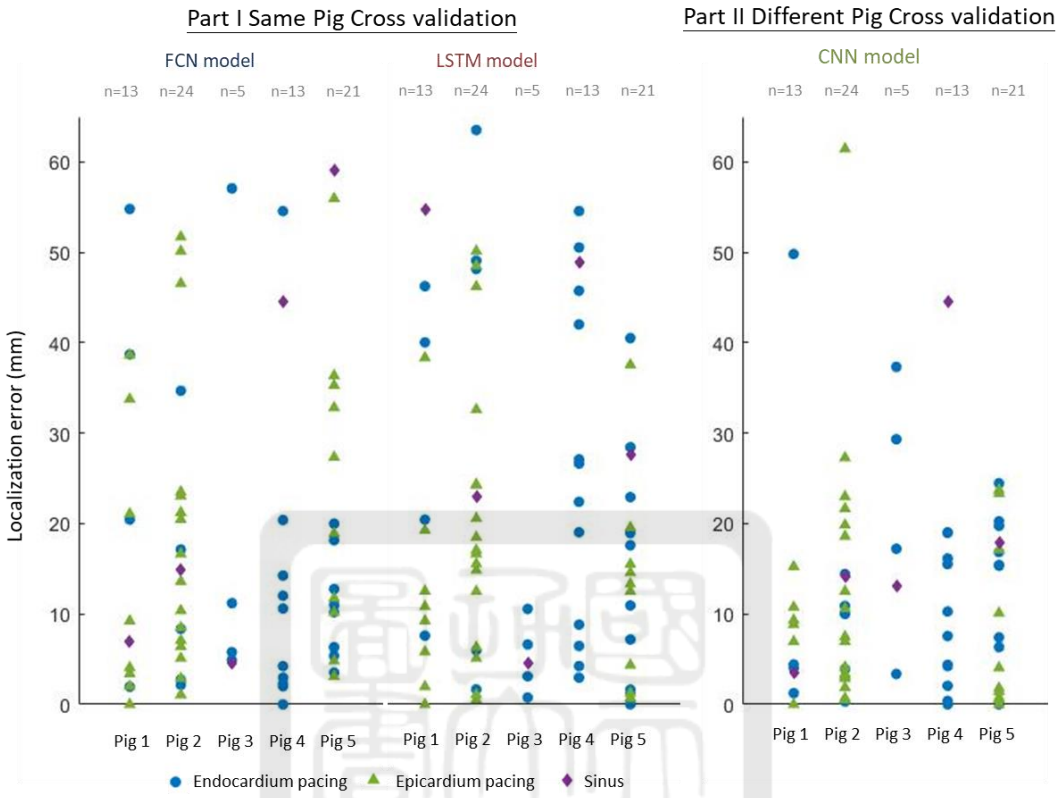

Figure 16, Localization error.

Chapter 4

Discussion, Conclusion and Future Works

4.1 Interpretation of the results

One of the main advancements in this study is solving the overfitting. Currently, neural networks have great flexibility to fit nearly all data types. However, a common problem is that the model cannot generalize to the data that the model has not seen. During our training, we observed that when using even a simple neural network with one fully connected layer, the model can converge to nearly obtain a correlation coefficient of 1. However, the overfitting problem always occurs.

In our dataset, the pattern of pacing has sufficient variability with the pacing site across all areas of the heart surface and endocardium. This probably explains why our results are much better than previous studies using neural networks. This may also explain the better results in part II that incorporate much more data with different pacing sites.

When viewing the result, we can see the variability between different pig and different recording varied greatly. For example, in part II study, the CNN model performs very well when cross validate on the pig 5, which shows correlation coefficient all above 0.8. However, in pig 2, some recording even shows negative correlation. This may be due to small date set. And the data set is not large enough to cover all the possible variability of the heart condition. Another observation is that when we compare the result from part I and part II. This can be explained by the fact that, in part II study, we incorporate data across different pig and greatly increase the training data.

4.2 Comparison with Previous Reported Accuracy

Most previous studies have median correlation coefficients of around 0.7. With a relatively simple model, we can achieve an overall correlation coefficient of around 0.74; see Table 2. This table is adapted from Table 2 in Bear et al.[5]. The results are presented as mean$\pm SD$ or median [interquartile range] *Only show the results from paced data. ** The results shown here are from the CNN model in this study.

Table 2 Comparison with Previous Studies for the Reconstruction of Epicardial Potential.

Subject type	Subjects	ECG cycles	Electrogram Correlation Coefficient	Localization Error mm	Activation Time Correlation Coefficient	Reference
Torso tank		4	>0.8	2-10		[1, 11]
Human	3	5	0.72±0.25	13±8		[12]
Human	4	79		13±9		[13]
Human*		6			0.68±0.17	[6]
Human	4	46		20.7[9.6–33.2]	0.71[0.65–0.74]	[14]
Dog	4	93	0.71[0.36–0.86]	10[7–17]	0.82	[15]
Pig	9	118		20.7[13.8–		[16]
Pig	5	70	0.72[0.40–0.84]	16[9–26]	0.78	[5]
Pig**	5	71	0.74[0.22–0.89]	9.3[3.4–17.0]	0.82[0.67–0.93].	This study

There are only five pigs, which means that the geometrical variance may not be sufficient to gain a better prediction. Considering that our data set is relatively small, this result is quite promising.

4.3 How important is the geometrical information?

We show that a rough geometrical transformation is sufficient for a model to make predictions. In the transformation of torso node information, the projection of nodes to the cylinder surface will definitely eliminate some information. For transformation of the heart node, the distortion is even greater and the registration did not consider the position of the heart in the body. However, the result shows that the information is sufficient to provide a model that can make predictions and avoid overfitting.

This result shows a possibility to avoid the need for geometric information. For example, we may use a standard torso body and heart as template for registration of electrode 3D location. When a new patient being tested, the electrode's position will then be registered by the standard body. And the predicted epicardial potential can than be view on the standard heart. With this work flow, we can avoid the need for performing CT or MRI examination. However, this will need a lot more study to realize.

4.4 Potential clinical application

The dataset we use in this study is epicardial pacing. The corresponding condition in disease will be premature ventricular contraction, which is also an abnormal excitation site from ventricle. This study shows the potential to identify the origin of premature ventricular activation from non-invasive recording of electrocardiogram of body surface. The information can be used to assist ablation site identification.

4.5 Limitations

Our dataset still has a limited scope; it did not contain rhythms such as atrial fibrillation, ventricular fibrillation, or ventricular premature beat. In addition, it did not contain data from hearts with scarring. Therefore, the model can only be applied to conditions such as sinus rhythm or epicardial pacing. This study only used four pigs. Pigs with significantly different geometry may show poor results.

4.6 Conclusions

A neural network can be used to solve the inverse problem of ECGi with relatively small datasets. Our best result shows overall median of the correlation efficient for the reconstructed epicardial potential to be 0.74. Our study also shows that a rough geometrical information of torso and heart may be enough to reconstruct the epicardial gram. Performance of the model is inconsistent between different recording and pig. This may be due to relatively small dataset and may improve with larger dataset. As shown in part II study, it has better result when model is trained with more data. In clinical setting, this study shows the potential to identify source of pacing site with non-invasive electro-cardiogram recorded from the surface, which can be apply to evaluation for patient with premature ventricular contractions.

References

[1] B. T. Howard S. Oster, Robert L. Lux, Philip R. Ershler, Yoram Rudy, "Noninvasive electrocardiographic imaging: reconstruction of epicardial potentials, electrograms, and isochrones and localization of single and multiple electrocardiac events.," *Circulation,* vol. 96, no. 3, pp. 1012–1024, 1997.

[2] D. H. B. Matthijs Cluitmans1, Rob MacLeod, Olaf Dössel, María S. Guillem,Peter M. van Dam, Jana Svehlikova, Bin He, John Sapp, Linwei Wang, Laura Bear, "Validation and Opportunities of Electrocardiographic Imaging: From Technical Achievements to Clinical Applications," *Front. Physiol,* vol. 9, p. 1305, 2018.

[3] P. S. C. Laura Bear, Olivier Bernus, Igor Efimov, Rémi Dubois, "Introduction to Noninvasive Cardiac Mapping," *Cardiac Electrophysiology Clinics,* vol. 7, no. P1-16, 2015.

[4] R. Y. Wang Y, "Application of the method of fundamental solutions to potential-based inverse electrocardiography," *Ann Biomed Eng,* vol. 34, pp. 1272-1288, 2006, doi: 10.1007/s10439-006-9131-7.

[5] L. R. Bear *et al.*, "How Accurate Is Inverse Electrocardiographic Mapping? A Systematic In Vivo Evaluation," *Circ Arrhythm Electrophysiol,* vol. 11, no. 5, p. e006108, May 2018, doi: 10.1161/CIRCEP.117.006108.

[6] S. F. Duchateau J, Pambrun T, Derval N, Chamorro-Servent J, Denis A, Ploux S, Hocini M, Jaïs P, Bernus O, et al., "Performance and limitations of noninvasive cardiac activation mapping," *Heart Rhythm,* vol. 16, pp. 435–442, 2019.

[7] L. S. Joe Horvath, Tommy Peng, Avinash Malik, Mark Trew, Laura Bear, "Deep learning neural nets for detecting heart activity," *arXiv:1901.09831 [physics.med-ph],* 2019.

[8] G. W. Aras K, Tate J, Burton B, Brooks D, Coll-Font J, Doessel O, Schulze W, Potyagaylo D, Wang L, van Dam P, MacLeod R. , "Experimental data and geometric analysis repository-EDGAR," *J Electrocardiol,* no. 48, pp. 975–981, 2015.

[9] C. L. Bear LR, LeGrice IJ, Sands GB, Lever NA, Paterson DJ, Smaill and BH., "Forward problem of electrocardiography: is it solved?," *Circ Arrhythm Electrophysiol.,* vol. 8, pp. 677–684, 2015.

[10] P. M. Duchateau J, Dubois R, "Spatially coherent activation maps for electrocardiographic imaging," *IEEE Trans Biomed Eng,* vol. 64, no. 5, pp. 1149 - 1156, 2017.

[11] "Noninvasive electrocardiogram imaging of substrate and intramural ventricular tachycardia in infarcted hearts," *J Am Coll Cardiol,* vol. 38, pp. 2071–2078, 2001.

[12] J. P. Ghanem RN, Ramanathan C, Ryu K, Markowitz A, Rudy Y, "Noninvasive electrocardiographic imaging (ECGI): comparison to intraoperative mapping in patients.," *Heart Rhythm,* vol. 2, no. 4, pp. 339-354, 2005.

[13] D. F. Sapp JL, Clements JC, Horácek BM, "Inverse solution mapping of epicardial potentials: quantitative comparison with epicardial contact mapping," *Circ Arrhythm Electrophysiol,* vol. 5, pp. 1001–1009, 2012.

[14] O. M. Graham AJ, Zacur E, Dhillon G, Daw H, Srinivasan NT, Lane JD, Cambridge A, Garcia J, O'Reilly NJ, Whittaker-Axon S, Taggart P, Lowe M, Finlay M, Earley MJ, Chow A, Sporton S, Dhinoja M, Schilling RJ, Hunter RJ, Lambiase PD, "Simultaneous comparison of electrocardiographic imaging and epicardial contact mapping in structural heart disease," *Circ Arrhythm Electrophysiol,* vol. 12, no. 11, 2019.

[15] P. P. B. P. Matthijs J.M.Cluitmans MD, Joël M.H.Karel PhD, MarcoDas MD,PhD, Bas L.J.H.Kietselaer MD, PhD Monique M.J. Jonga Frits W.Prinzen PhD, Ralf L.M.PeetersPhD. Ronald L.Westra PhD, Paul G.A.Volders MD, PhD, "In Vivo Validation of Electrocardiographic Imaging," *JACC Clin Electrophysiol*, vol. 3, no. 3, pp. 232-242, 2017.

[16] M. E. R. Stephan Hohmann, Hiroki Konishi, Anna Borenstein, Songyun Wang, Atsushi Suzuki, Gregory J. Michalak, Kristi H. Monahan, Kay D. Parker, L. Katie Newman, Douglas L. Packer, "Spatial Accuracy of a Clinically Established Noninvasive Electrocardiographic Imaging System for the Detection of Focal Activation in an Intact Porcine Model," *Circulation: Arrhythmia and Electrophysiology*, vol. 12, no. 11, 2019.